Modeling of Wrinkle Formation in Non-Crimp Dry Fabric during Preform Compaction

Von Jamora, Benjamin Laredo, Oleksandr Kravchenko
Old Dominion University, Norfolk, Virginia, 23508

Abstract

Lightweight components in the automotive industry need to be draped into complex parts during liquid molding. Composite dry fabric can develop wrinkles and fiber waviness during the preform compaction stage. As a result, the compaction of the textile can result in defects, such as wrinkling which affect the local fiber volume fraction variation. Therefore, to simulate the compaction of the dry quadaxial non-crimp fabric, a finite element analysis (FEA) framework was developed. The custom material subroutine was made to simulate the non-linear deformation of dry fabric preform. The constitutive material model used the superposition of an elastic and a viscous component. The elastic part used an isotropic hyperelastic behavior, and the viscous part was composed of a strain and a strain rate dependent element, which are functions of the fiber volume fraction and compaction speed, respectively. The stress-strain response from a unidirectional compaction test, with varying compaction speeds, was used to define the viscous behavior. The FEA model of wrinkle formation due to the cylindrical roller compaction shows a close correlation with the experimental test demonstrated in the stress strain behavior. Results of the analysis demonstrate the fiber volume fraction varies through the thickness and voids can be seen forming due to the wrinkling between layers.

Introduction

The automotive industry needs lightweight materials to reduce fuel consumption while maintaining strength and cost. Many of these automotive components also need to be manufactured into complex shapes. Such parts include the chassis, wheels, and seat backs to name a few. Composites are a type of material widely used in the industry with numerous forms and manufacturing methods. A common configuration for these composite materials is dry woven fabrics such as non-crimp fabric (NCF). NCFs are multiple layers of unidirectional fibers but vary in orientations from layer to layer. The multiple layers are stitched together with different materials such as nylon to create a quasi-isotropic configuration. The absence of crimping in the fabric means the fiber remains consistently straight for every layer which maintains the mechanical properties of the unidirectional fibers. The drapeability of the composite allows for the fabric to be molded into complex shapes before resin infusion. NCFs allows for a good combination of the superior properties of continuous fibers with the ease of use of textile composites. Another benefit for NCFs is that the lack of matrix in the dry fabric allows for long storage times [1].

The manufacturing process for dry fabrics involves infusing resin into the dry fabric preforms. These methods include resin transfer molding (RTM) and liquid composite molding. Furthermore, there are variations in these processes such as differing pressures for the RTM or using a vacuum to assist the resin through the weave. These infusion methods typically involve a mold that shapes the fabric into the component. However, the compression of dry woven fabric could result in wrinkling or the fiber orientation being shifted before resin infusion [2]. Residual stresses are prevalent in the manufacturing process, and this can be perpetuated by defects during the stitching. So, maintaining the dimensional stability of the fabric is important for NCFs [3]. Therefore, it is important to predict the final morphology and the fiber distribution of the NCF during compression.

Dry fabric needs to be infused with resin and cured. This means the permeability of the resin is an important factor for the manufacturing process of any textile-based composites structures. Studies have shown that the resin infusion behavior changes when the fabric is deformed [4]. An important property to determine is the fiber volume fraction throughout the structure since it is shown that the permeability through the fibers is directly related to the fiber volume fraction, it is valuable to predict the initial volume fraction [5], [6]. Furthermore, the mechanical properties of the composite are also directly influenced by the fiber volume fraction [7]. Overall, it is crucial to know the fiber volume fraction of the NCF to predict the resin flow through the laminate.

An analytical equation exists to predict the fiber volume fraction of non-crimp fabrics. However, this solution homogenizes the fabric and cannot determine the distribution of the fiber volume fraction through the dry fabric. This demonstrates the need for better method needs to determine the fiber volume fraction distribution of a quadaxial non-crimp fabric. Furthermore, constitutive models for plain weave fabric exist which can be applied to non-crimp fabric. The proposed method is to simulate the compaction of the fiber through finite element analysis (FEA) using Abaqus with a custom VUMAT subroutine to simulate a fiber volume fraction dependent apparent viscosity of a non-crimp fabric. The VUMAT uses a superposition of an elastic and viscous components, where the viscous components are composed of a strain and a strain rate dependent term. The FEA model will establish the distribution of the fiber volume fraction through the thickness of the compacted composites.

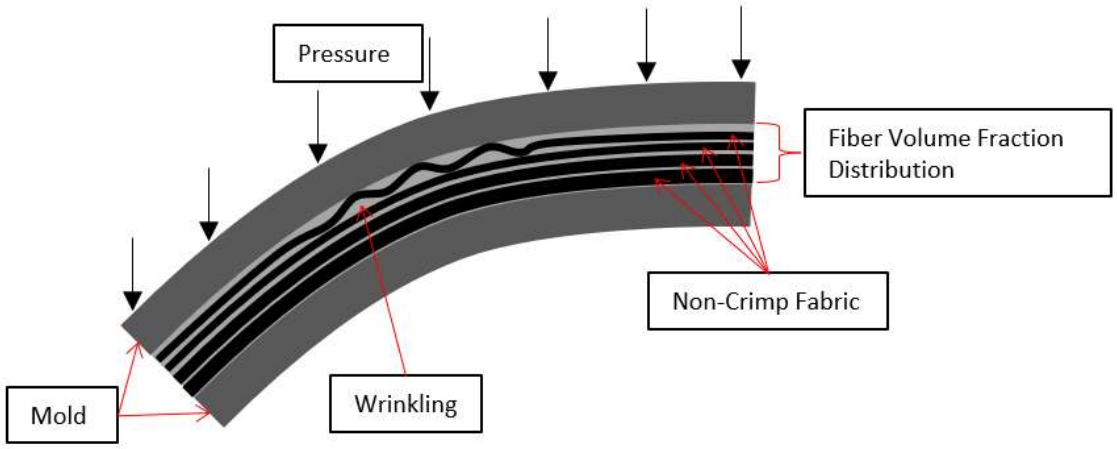

Figure 1. A presser foot is used on fabric placed on a convex tool shape. Where wrinkling is present in the front due to the presser foot

METHODOLOGY

The material used in the compaction experiment is Saertex multiaxial non-crimp fabric with a layup configuration of [+45/-45/0/90/0/-45/+45] where the layers are held together by a polymer thread. The compaction data used in the modeling was derived from the work of Laredo [2]. The compaction data consisted of a combination of tests with varying dimensions, thickness, and compaction speeds. The dimensions were 152 x 152 mm and 229 x 229 mm fabric, and the thickness was 4- and 8-mm thick, where each layer was 2 mm. For the compaction test, the speed used were 1, 2, and 5 mm/min. Curves from the five experiments are used to fit a curve for the apparent viscosity of the non-crimp fabric compaction simulation [2]. The mechanical properties of the fiber are derived from literature for the carbon fiber Zoltek PX35, which has properties shown in table 1 [8].

Table 1. Properties for Zoltek PX35	
Tensile Modulus	242 GPa
Density	1.81 g/cc

Although the fabric consists of seven layers of composites stitched together, the simulation homogenizes the fabric into one element as depicted in figure 2. A laminate that is 8 mm thick, would consist of four layers of quadaxial fabric which translates to four elements through the thickness for the FEA model.

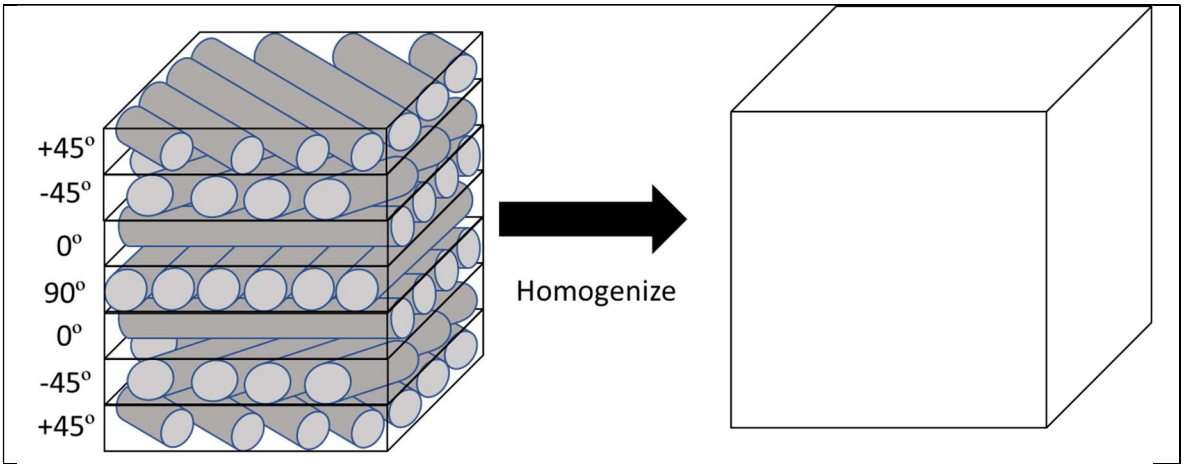

Figure 2. Homogenization of multiple layers into one element for each laminate of dry fabric

Finally, the roller is used to compact the composite weave, using a Tinius Olsen 10ST universal testing machine. The roller is assumed to be steel with the properties of the young's modulus of 215 GPa, a Poisson's ratio of 0.3, and a density of 7.85 g/cc. The tip of the roller is 5 mm in diameter with a width of 30 mm.

For the finite element modeling of the compaction of composites, the proposed constitutive model consists of two components, an elastic, and a viscous component as shown in equation 1.

$$\hat{\sigma} = \hat{\sigma}_e + \sigma_v ii, i = 3 \quad \text{Eq. 1}$$

The elastic model is derived from an isotropic hyperelastic constitutive equation which will simulate the elasticity of the fibers [9]. The equation uses neo-Hookean hyperelasticity calculated from the invariants of the left Cauchy-Greene strain tensor which is shown in equation 1.

$$\sigma_{e\,ii} = \frac{\mu}{J}\left(\hat{B} - \hat{I}\right) + \lambda(J-1)\hat{I}, ii = 1{,}2 \quad \text{Eq. 1}$$

Where $\hat{B}$ is the left Cauchy-Green Strain Tensor derived from the deformation gradient, $\hat{I}$ is the identity matrix, and J is the determinant of the deformation gradient. The μ and λ are the lame constants of the fiber [10]. It can be noted that equation 1 only includes the x and y-directions or the two fiber dominated axes. For simplicity, each laminate is homogenized due to the quasi-isotropic stacking sequence

For the apparent viscosity of the non-crimp fabric compaction, a solution for plain weave fabric is proposed by Kelly, where the viscous component is a multiplicative term that further consists of two components. The same principles can be applied to non-crimp fabric for a finite element model. An apparent viscosity can be used for stress calculations for the

compressive stress which will consists of a strain-dependent and strain-rate-dependent term. The solution uses the fiber volume fraction as the strain variable and the compaction speed is used as the strain rate variable as shown in equation 2 [11].

$$\sigma_{33} = \sigma_v(V_f, v) = \sigma_\beta(V_f)\sigma_\alpha(v) \quad \text{Eq. 2}$$

The two functions are fitted using the compaction experiment data. The parameters for functions were fitted using the nonlinear curve fit available in MATLAB. For the strain fiber volume fraction dependent term, a polynomial equation is fitted shown in equation 3.

$$\sigma_\beta(V_f) = \beta_1^{\beta_2 * vf - \beta_3} + \beta_4 \quad \text{Eq. 3}$$

Where the V_f^{dat} is a reference fiber volume fraction at some nominal stress, β_0 taken from a single experiment. In this case, the data was fitted at middle compaction speed of 2 mm/min of a 152 x 152 mm, 4 mm thick laminate as the reference. The compaction curve for this experiment is shown in figure 3. The parameters derived from the 2 mm/min compaction curve from the plot are shown in table 2, where it is shown, the function is well correlated to the experimental plot.

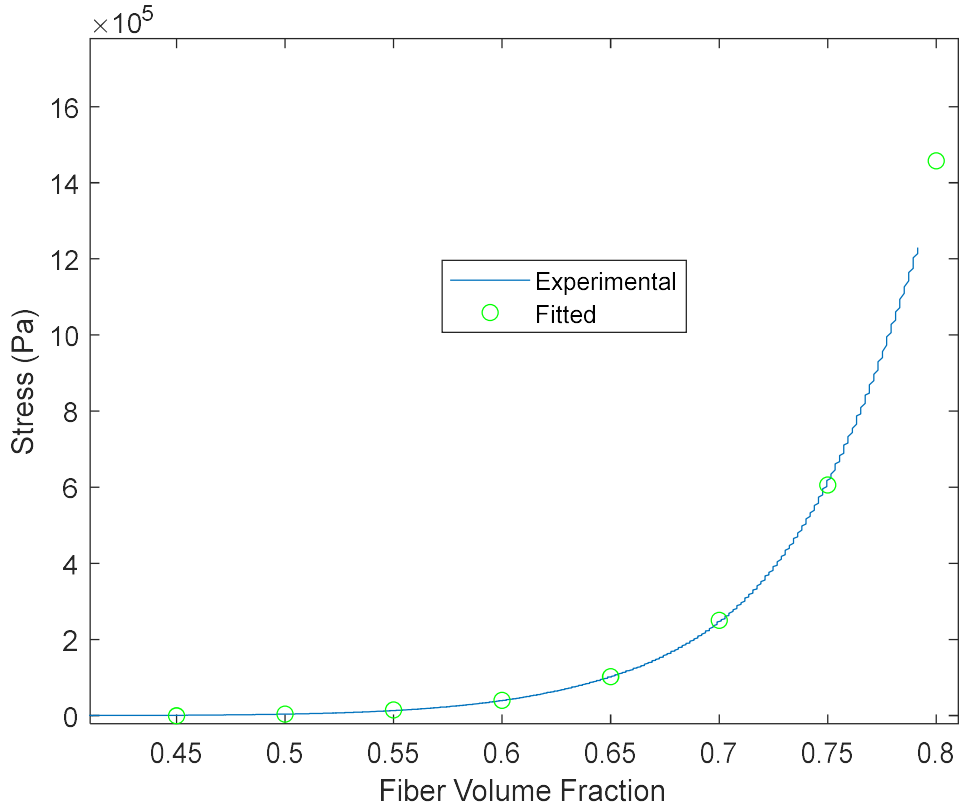

Figure 3. The compaction curve of 152 x 152 mm, 2 laminates, at 2 mm/min compaction speed with respect to the fiber volume fraction.

As for the strain rate dependent equation, data points from a reference volume fraction and used the data from various compaction speeds. A reference volume fraction of 0.60 was chosen to fit the functions for the strain rate, or compaction speed dependent data. The data points shown in figure 4 are used to fit the function shown in equation 4.

$$\frac{\sigma(v)}{\sigma(0)} = \frac{\sigma(\infty)}{\sigma(0)} - \left[\alpha_1 \left(\frac{v}{v_{ref}}\right)^{\alpha_2} + \left(\frac{\sigma(\infty)}{\sigma(0)} - 1\right)^{-\alpha_3}\right]^{\frac{1}{\alpha_3}} \qquad \text{Eq. 4}$$

Where $\sigma(0)$ is the lowest stress taken from the lowest speed (1 mm/min) and $\sigma(\infty)$ is the largest stress at he fastest speed (5 mm/min). v_{ref} is the compaction speed at the middle of the two extremes (2 mm/min). The fitted parameters, $\alpha_1, \alpha_2 \alpha_3$, $\sigma(0)$ and $\sigma(\infty)$are shown in table 2

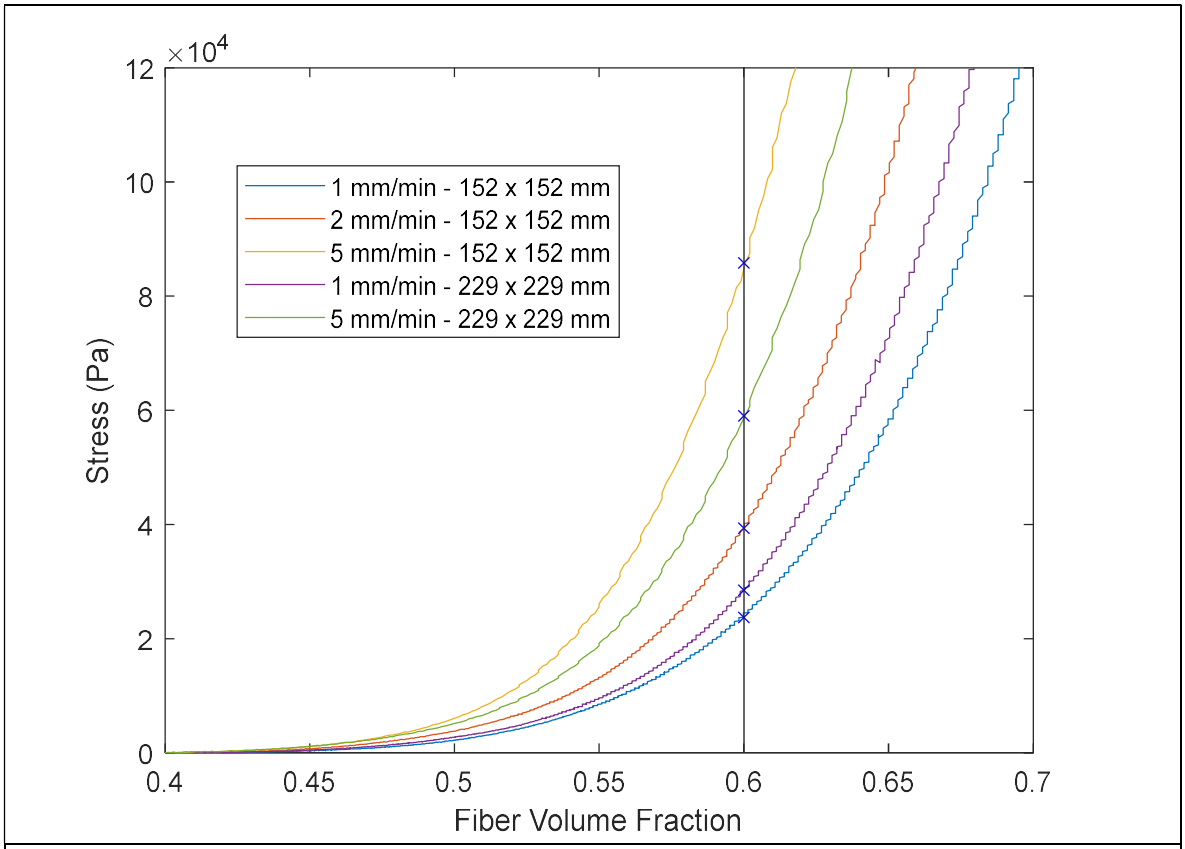

Figure 3. The compaction curves were used for the strain rate-dependent analysis.

Table 2. Fitted parameters for the composite material used in the work			
β_1	9.6605E4 Pa	α_1	0.1254
β_2	1.5238 Pa	α_2	3.2054
β_3	-0.0176 Pa	α_3	1.6507
β_4	-2.254E3 Pa	$\sigma(\infty)$	8.5829e4 Pa
V_f^{dat}	0.60	$\sigma(0)$	2.3726e4 Pa
		v_{ref}	2

As the material is compressed the fibers in the weave is compacted. Consequently, this increases the fiber volume fraction and influences the apparent viscosity which means the fiber volume fraction needs to be updated pr time step. The initial fiber volume fraction can be calculated using equation 4.

$$V_{f_0} = \frac{\rho_a n}{\rho_f T} \quad \text{Eq. 4}$$

where ρa is the areal density of the fabric, n is the number the laminate in the sample, ρf is the density of the specific fiber, and T is the thickness of the sample [2]. For these laminates, ρa=1425 g/m^2, ρf=1.79*10^6 g/m^3, and n = 1 since the fiber volume fraction is calculated for each layer. The fiber volume fraction can then be updated for each time step using equation 5 [12].

$$V_f = V_{f_0} e^{\varepsilon} \quad \text{Eq. 5}$$

Where ε is the strain directly provided from the subroutine and V_f is the fiber volume fraction at the time step.

A single element model was used to test the fiber volume fraction based constitutive model, which consisted of a single C3D8R element. Three different velocities were used, which coincides with the experimental compaction speeds. The different speeds were applied through a displacement boundary condition at the top and constrained at the bottom to simulate a tool during compaction.

A more complex model was simulated for the compaction of an 8mm thick (4 laminates) with varying compaction speeds which are 1 mm/min for 30 seconds. For the non-crimp fabric each deformable solid used to represent the laminates were meshed with 27094 C3D8R elements with one element through the thickness for each non-crimp layer. A schematic of the compaction model is shown in figure 4. The non-crimp fabric is constrained vertically at the z-direction to simulate the tool and a deformable solid was used to simulate the roller. A mass scaling of 5 was applied a

faster completion time. A frictionless boundary condition was applied to the surface between the laminate layers and the roller.

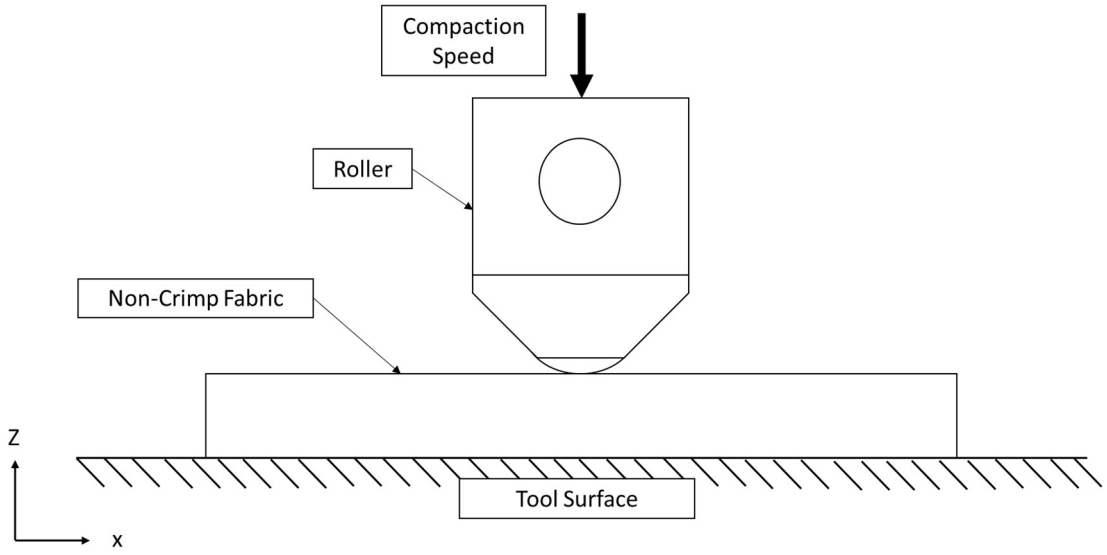

Figure 4. The schematic of the roller compaction model

Results

The single element tests show good correlation between the numerical solution and the experimental data in terms of stress vs strain (fig. 5). Deviation can be seen for the 5 mm/min, but the 1 mm/min and the 2 mm/min results show fitting results. This shows that the model is capable of simulating the stress experienced by a non-crimp fabric at different compaction speeds. Furthermore, the model this proves that the model which has been previously used for plain-weave fabric can simulate the compaction of a non-crimp fabric. Since the fiber volume fraction is directly related to the strain, the model is capable of predicting the variable at a large range of strain. Consequently, the model can be utilized for more complex FEA simulations which involves a physical roller.

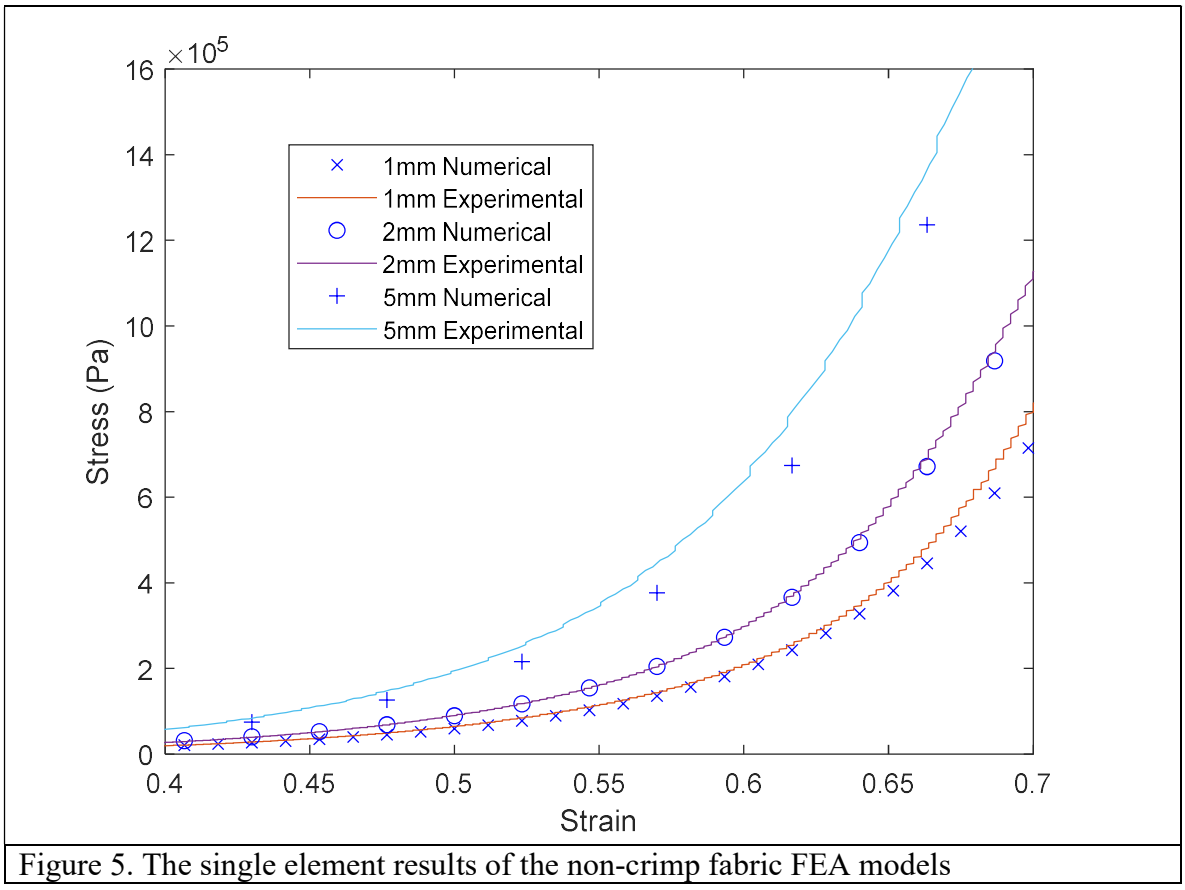

Figure 5. The single element results of the non-crimp fabric FEA models

The model shows distribution of fiber volume fraction through the thickness of the four layers of non-crimp fabric in the z-y plane (fig. 6). Expectedly, the fiber volume fraction is greater on top and decreases as towards the bottom. Furthermore, the fiber volume fraction is concentrated near the roller where it radiates outwards from the center where the compaction occurs. These gradients show that permeability during resin infusion may be affected by the different fiber volume fraction distribution throughout the model. The maximum fiber volume fraction calculated was 42.3% at a deformation of 0.50 mm through the thickness. In comparison, the 1 mm/min experimental data shows a calculated value of 46.6% for the fiber volume fraction. This shows a percent difference of 9.67%. This shows the potential for the model to simulate complex non-linear deformation of non-crimp fabrics.

Furthermore, at the X-Z plane cross section of the FEA model, the waviness can be seen at the layers of the non-crimp fabric early in the compaction. This waviness propagates further in the compaction process and create voids and resin rich regions. These areas allow for defects to occur and reduce the overall strength of the composite properties [13]. Such compaction signatures should be considered when manufacturing with non-crimp fabric. It can be seen that the further in the x-direction, the compaction of the roller impacts the fiber

volume fraction of the neighboring fabric. Overall, the model shows a good capability of demonstrating the differences in fiber volume fraction and deformation in non-crimp fabric. The winkling phenomenon in the model shows the importance of predicting the final morphology of non-crimp fabrics.

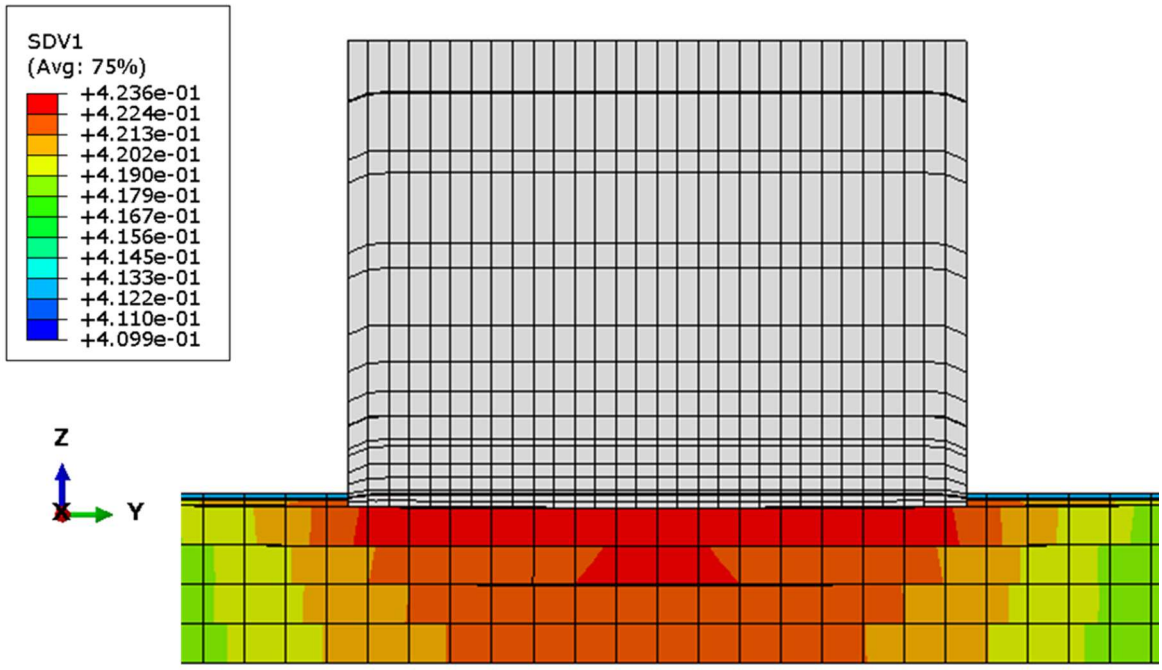

Figure 6. The fiber volume fraction distribution of the non-crimp fabric simulation with a velocity of 1 mm/min

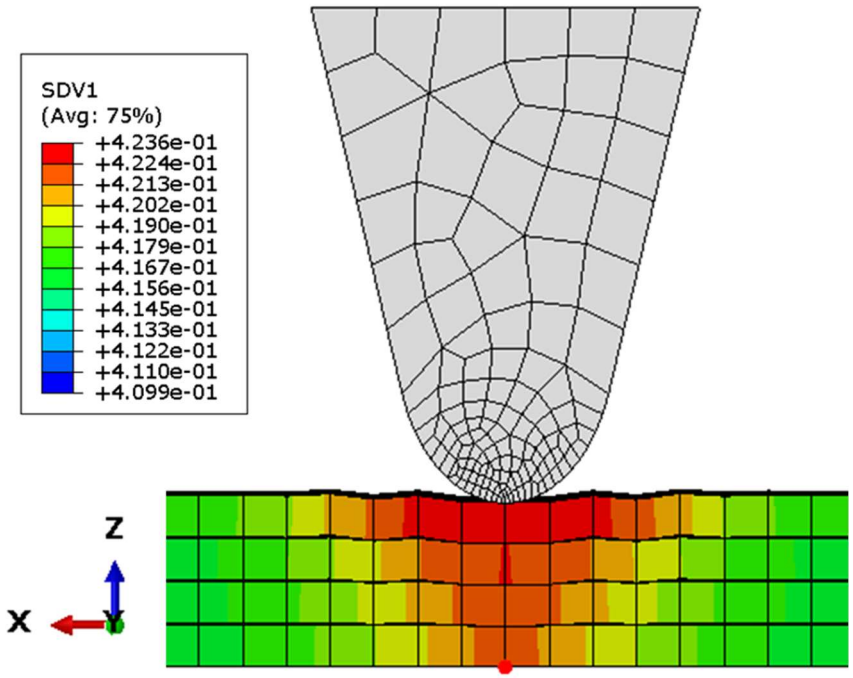

Figure 7. The Z-X plane view of the model, which depicts the waviness in the non-crimp fabric.

Conclusion

A model was made with a hyperelastic component and a viscous component. The viscosity component consisted of a fiber volume fraction and a compaction speed dependent term. Parameters for the apparent viscosity was derived from multiple compaction experiments. The simulation done for three compaction speeds of a single element non-crimp fabrics. Results show the model is capable of simulating the stress strain response of a non-crimp fabric with a fiber volume fraction-based for all three of the different velocities applied. This indicates the model can properly simulate the compaction of a non-crimp fabric.

The more complex roller compaction was able to simulate a distribution of fiber volume fraction through the thickness. The maximum fiber volume fraction shown in the model was very similar to the measured fiber volume fraction of the measured fiber volume fraction of the experimental work. The model also depicted a wrinkling phenomenon in the early stages of the compaction. This indicates that the waviness could propagate when more deformation is applied to the non-crimp fabric. This means that voids and resin rich regions could directly result from the compaction of these non-crimp fabrics, and non-linear signatures such as these should be taken into account when infusing non-crimp fabrics.

Future Work

While the amount of displacement the model was subjected to was small, the model can be improved further to allow for longer simulations. There are different approaches to further simulate the compaction of the non-crimp fabric more realistically. For example, each layer of the non-crimp fabric can be modeled instead of a homogenous laminate where the fiber orientation can then be varied for each layer based on the stacking sequence of the fabric. More complex analyses may also model the effects of different stitching material. A sensitivity analysis can also be performed to observe the effects of the finite element analysis parameters and geometry. Similar to the single element models, different compaction speed will be applied to the complex roller model. Better metrics will be used to measure the accuracy of the model, such as the reaction force of the roller.

Furthermore, a wrinkling test can be done to simulate the stress relaxation to simulate the effects when the force is released. Any hysteresis can then be quantified through the permanent change in fiber volume fraction. Furthermore, the roller can be moved through the surface of the non-crimp fabric to seem the wrinkling affects processes such as stitching could have on the material. This would simulate any defects present in the material before the resin infusion process.

Acknowledgements

Von Jamora is Acknowledging support from NSF scholarship in STEM (Award # 1833896)

References

[1] P. K. Mallick, *Processing of Polymer Matrix Composites*. New York: CRC Press, 2017. doi: 10.1201/9781315157252.

[2] A. Beltran Laredo, "Mechanism of Compaction With Wrinkle Formation During Automatic Stitching of Dry Fabrics and the Size Effect of Compression Molded Discontinuous Fiber-Reinforced Composites," *Mech. Aerosp. Eng. Theses Diss.*, Aug. 2020, doi: 10.25777/e2bb-b036.

[3] W. Chen, D. Zhang, X. Ren, and J. Lua, "A Coupled Flow and Residual Stress Model for Predicting Performance Variations of Composites Manufactured via Vacuum Assisted Resin Transfer Molding," in *AIAA Scitech 2020 Forum*, American Institute of Aeronautics and Astronautics, 2020. doi: 10.2514/6.2020-2111.

[4] J. I. Kim, Y. T. Hwang, K. H. Choi, H. J. Kim, and H. S. Kim, "Prediction of the vacuum assisted resin transfer molding (VARTM) process considering the directional permeability of sheared woven fabric," *Compos. Struct.*, vol. 211, pp. 236–243, Mar. 2019, doi: 10.1016/j.compstruct.2018.12.043.

[5] J. Westhuizen and J. P. D. Plessis, "Quantification of Unidirectional Fiber Bed Permeability," *J. Compos. Mater.*, vol. 28, no. 7, pp. 619–637, May 1994, doi: 10.1177/002199839402800703.

[6] Y. R. Kim, S. P. McCarthy, J. P. Fanucci, S. C. Nolet, and C. Koppernaes, “Resin flow through fiber reinforcements during composite processing,” *SAMPE Q. Soc. Aerosp. Mater. Process Eng. U. S.*, vol. 22:3, Apr. 1991, Accessed: Dec. 15, 2021. [Online]. Available: https://www.osti.gov/biblio/5470988

[7] J. Song, W. Wen, H. Cui, H. Liu, and Y. Xu, “Effects of temperature and fiber volume fraction on mechanical properties of T300/QY8911-IV composites,” *J. Reinf. Plast. Compos.*, vol. 34, no. 2, pp. 157–172, Jan. 2015, doi: 10.1177/0731684414565939.

[8] “ZOLTEK™ PX35 Multi-Directional Fabrics.” [Online]. Available: https://zoltek.com/wp-content/uploads/2017/09/TDS_PX35_MD_Fabrics.pdf

[9] J. P.-H. Belnoue, O. J. Nixon-Pearson, D. Ivanov, and S. R. Hallett, “A novel hyper-viscoelastic model for consolidation of toughened prepregs under processing conditions,” *Mech. Mater.*, vol. 97, pp. 118–134, Jun. 2016, doi: 10.1016/j.mechmat.2016.02.019.

[10] J. Bonet and A. J. Burton, “A simple orthotropic, transversely isotropic hyperelastic constitutive equation for large strain computations,” *Comput. Methods Appl. Mech. Eng.*, vol. 162, no. 1, Art. no. 1, Aug. 1998, doi: 10.1016/S0045-7825(97)00339-3.

[11] P. A. Kelly, “A viscoelastic model for the compaction of fibrous materials,” *J. Text. Inst.*, vol. 102, no. 8, pp. 689–699, Aug. 2011, doi: 10.1080/00405000.2010.515103.

[12] P. Kelly, R. Umer, and S. Bickerton, “Compaction of dry and wet fibrous materials during infusion processes,” 2004, vol. 36, pp. 785–797.

[13] A. Trochez, D. Ghosh, K. C. Wu, V. C. Jamora, and O. Kravchenko, “Effects of Automated Fiber Placement Defects on High Strain Rate Compressive Response of Advanced Composites,” *Submitt. Compos. Mater.*, 2021.